Liang et al. Nanoscale Research Letters (2016) 11:505
DOI 10.1186/s11671-016-1720-2

Nanoscale Research Letters

NANO EXPRESS Open Access

Visible photoassisted room-temperature oxidizing gas-sensing behavior of Sn_2S_3 semiconductor sheets through facile thermal annealing

Yuan-Chang Liang*, Tsai-Wen Lung and Chein-Chung Wang

Abstract

Well-crystallized Sn_2S_3 semiconductor thin films with a highly (111)-crystallographic orientation were grown using RF sputtering. The surface morphology of the Sn_2S_3 thin films exhibited a sheet-like feature. The Sn_2S_3 crystallites with a sheet-like surface had a sharp periphery with a thickness in a nanoscale size, and the crystallite size ranged from approximately 150 to 300 nm. Postannealing the as-synthesized Sn_2S_3 thin films further in ambient air at 400 °C engendered roughened and oxidized surfaces on the Sn_2S_3 thin films. Transmission electron microscopy analysis revealed that the surfaces of the Sn_2S_3 thin films transformed into a SnO_2 phase, and well-layered Sn_2S_3–SnO_2 heterostructure thin films were thus formed. The Sn_2S_3–SnO_2 heterostructure thin film exhibited a visible photoassisted room-temperature gas-sensing behavior toward low concentrations of NO_2 gases (0.2–2.5 ppm). By contrast, the pure Sn_2S_3 thin film exhibited an unapparent room-temperature NO_2 gas-sensing behavior under illumination. The suitable band alignment at the interface of the Sn_2S_3–SnO_2 heterostructure thin film and rough surface features might explain the visible photoassisted room-temperature NO_2 gas-sensing responses of the heterostructure thin film on exposure to NO_2 gas at low concentrations in this work.

Keywords: Semiconductor, Sheets, Crystal feature, Surface, Gas-sensing response

Background

Binary tin sulfide semiconductors, because of their narrow band gap values and *n*-type semiconducting characteristics, have attracted considerable attention in applications of various photovoltaic and photoactivated devices [1–4]. For practical scientific applications, tin sulfide semiconductors in the form of a thin-film structure are in high demand. Several synthesis techniques, such as spray pyrolysis [3], thermal evaporation [4], chemical bath deposition [5], and chemical vapor deposition [6], have been successfully employed in preparing tin sulfide semiconductor thin films. Sputtering thin-film preparation methods are frequently used to fabricate complex compounds in the semiconductor industry because they enable easy process control, large area deposition, feasibility with a wide range of thin-film thickness, and high reproducibility [7–9]. However, few reports on thin-film synthesis of tin sulfide semiconductors through sputtering techniques have been published.

Resistive gas sensors are crucial in industrial and medical applications for detecting pollutants as well as toxic and combustible gases. Growing interest has inspired the development of diverse gas sensors used at low temperatures or in room-temperature environments [10]. However, overcoming high barriers is generally necessary for the gas molecules to adsorb onto and desorb from the semiconductor surfaces during gas-sensing response and recovery at low temperatures; therefore, fabricating thin-film semiconductor-based gas sensors that have visible gas-sensing behaviors at room temperature remains a considerable challenge. Moreover, narrow band gap tin sulfide semiconductors have rarely been reported for applications in gas-sensing materials operated at room temperature. Recently, various heterostructures have been widely investigated and show enhanced functions of the

* Correspondence: yuanvictory@gmail.com
Institute of Materials Engineering, National Taiwan Ocean University, Keelung 20224, Taiwan

single constituent counterpart [11–13]. Moreover, a novel concept of sensing mechanisms, such as gas sensing based on the variation in the photoelectric response, was proposed [14]. Photoexcited carriers were shown to be crucial for improving the gas-sensing responses of semiconductor-based sensors operated at a low room temperature [15]. Several heterostructure systems such as TiO_2–CdS and SnO_2–ZnO exhibit clear reducing and oxidizing gas-sensing properties, respectively, under light illumination at room temperature [16, 17]. In the present study, tin sulfide thin films with a sheet-like surface were synthesized through radiofrequency (RF) sputtering. The as-synthesized tin sulfide thin films exhibited a visible gas-sensing response to low-concentration NO_2 gases under light illumination at room temperature when the films were subjected to a simple postthermal annealing procedure. The correlation between the tin sulfide thin film microstructures and oxidizing gas-sensing properties was initially investigated in this study.

Methods

In this study, the preparation of Sn_2S_3–SnO_2 heterostructure thin film consists of two steps. First, Sn_2S_3 thin films were fabricated onto 300-nm-thick SiO_2/Si substrates using RF magnetron sputtering. SnS_2 ceramics target was used to sputtering growth Sn_2S_3 thin film which has a nonstoichiometric composition from the target material. During the growth of Sn_2S_3 thin film, the sputtering power of SnS_2 target was fixed at 40 W. The thin-film growth temperature of the Sn_2S_3 thin films was maintained at 250 °C in pure Ar ambient; the gas pressure during the sputtering thin-film deposition was fixed at 0.67 Pa in this work. Subsequently, the as-grown Sn_2S_3 thin films were subjected to a postannealing procedure at 400 °C for 40 min in ambient air. This process engendered the surfaces of the Sn_2S_3 thin films oxidized and form the thin SnO_2 crystallites on the surfaces of the Sn_2S_3 thin films.

Thin-film crystal structures were investigated by X-ray diffraction (XRD; Bruker D2 PHASER) using Cu Kα radiation with a theta-two theta scan mode. The surface morphology of the samples was investigated by scanning electron microscopy (SEM; Hitachi S-4800). The detailed microstructures of the as-synthesized samples were characterized by high-resolution transmission electron microscopy (HRTEM; Philips Tecnai F20 G2). The composition analysis was performed using an energy-dispersive X-ray spectrometer (EDS) attached to the TEM. To measure NO_2 gas-sensing properties of the Sn_2S_3 and Sn_2S_3–SnO_2 thin films, the Pt interdigital electrodes were patterned onto the substrates by DC sputtering. Subsequently, the Sn_2S_3 and Sn_2S_3–SnO_2 thin films were prepared onto the Pt electrodes-coated substrates to form gas sensor devices. The gas-sensing measurements of the sensor were conducted at 5 V. A 100-W Xe arc lamp was used as the illumination source for light-assisted gas-sensing tests. The gas-sensing tests were conducted with various concentrations of NO_2 gas (0.2, 0.5, 1.0, and 2.5 ppm) at room temperature. The gas-sensing response of the sensor to NO_2 gas is defined as the Rg/Ra. Ra is the sensor electrical resistance in the absence of target gas and Rg is that in the target gas. The gas-sensing response of the sensor to 100 ppm CO, H_2, and NH_3 gases is defined as the Ra/Rg.

Results and Discussion

Figure 1a, b shows the morphologies of the sputtering-deposited Sn_2S_3 thin films with and without postannealing in ambient air. Fig. 1a shows that the surface of the Sn_2S_3 film has a visible sheet-like texture. These sheet-like crystallites had a sharp periphery and homogeneously covered the film surface. The size of the sheet-like surface crystallites ranged 150–300 nm. A similar sheet-like surface morphology was also reported for Sn_2S_3 thin films synthesized using a chemical solution method [5]. The periphery of the sheet-like Sn_2S_3 became rough and passivated after the postannealing procedure. Such a transformation in the morphology of a solid thin-film surface after various postannealing procedures has been attributed to factors such as the phase changes, the composition changes, or the growth of the grain size during postannealing procedures [18, 19]. Figure 2a, b shows XRD patterns of the Sn_2S_3 thin film with and without a postannealing procedure. Figure 1c shows three marked Bragg reflections centered at approximately 26.5°, 30.7°, and 31.7°. These Bragg

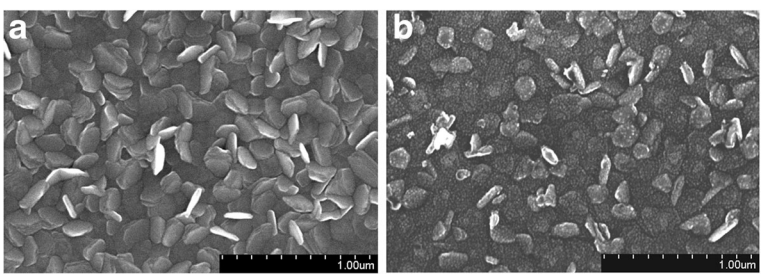

Fig. 1 SEM images. **a** Sn_2S_3 thin film. **b** Sn_2S_3–SnO_2 thin film

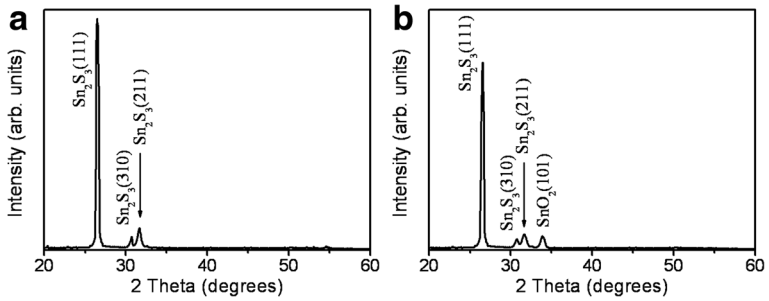

Fig. 2 XRD patterns. **a** Sn_2S_3 thin film. **b** Sn_2S_3–SnO_2 thin film

reflections originated from the (111), (310), and (211) crystallographic planes of the orthorhombic Sn_2S_3 (JCPDS No. 14-0619). The XRD result indicated that the Sn_2S_3 thin film mainly consisted of highly (111)-oriented grains. The XRD pattern showed that when the Sn_2S_3 thin film was postannealed in ambient air, it still exhibited a highly (111)-preferential orientation. Moreover, a visible Bragg reflection of SnO_2 (101) appears in Fig. 2b (JCPDS No. 88-0287), confirming the formation of Sn_2S_3–SnO_2 heterostructure thin film with a high crystallinity.

Figure 3a shows a low-magnification cross-sectional TEM image of the Sn_2S_3–SnO_2 heterostructure thin film. The TEM image revealed that the film had an undulated surface morphology. The surface of the film was considerably rugged. The drop height of the surface protrusions evaluated from the TEM image ranged approximately 100–150 nm. Figure 3b shows a HRTEM image taken from the internal region of the Sn_2S_3–SnO_2 heterostructure (region 1 marked in Fig. 2a). Ordered and clear lattice fringes were observed in the HRTEM image, revealing that the film had a high crystallinity. Moreover, the local lattice fringes with an interval of approximately 0.335 nm corresponded to the interatomic distance of orthorhombic Sn_2S_3 (111). The HRTEM image taken from the outer region (region 2 marked in Fig. 3a) of the film is shown in Fig. 3c. Clear and ordered lattice fringes with intervals of approximately 0.335 nm corresponded to orthorhombic Sn_2S_3 (111), and the lattice fringes with an interval of approximately 0.264 nm in the outer region matched the spacing distance of

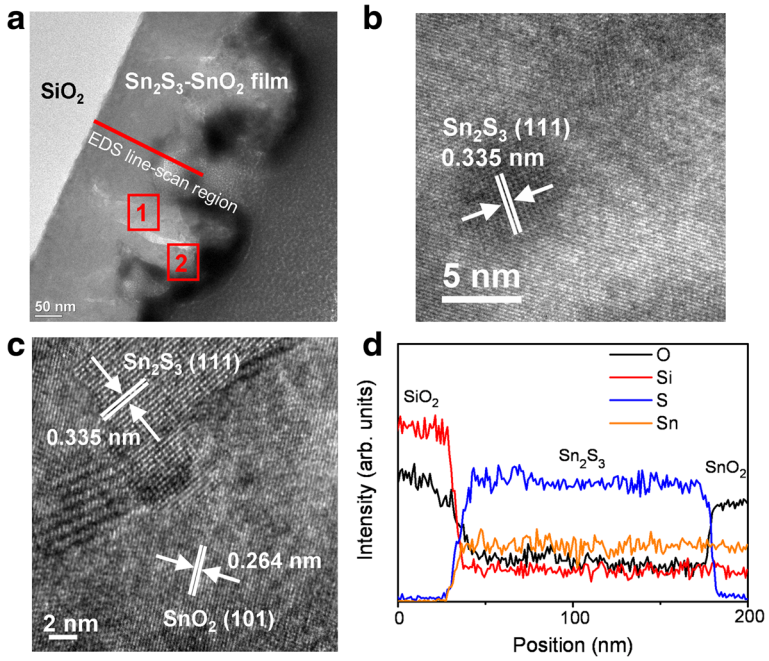

Fig. 3 TEM analyses of the Sn_2S_3–SnO_2 thin film. **a** Low-magnification cross-sectional TEM image of the film. **b** HRTEM image taken from the inner region of the film (marked with *1* in **a**). The region corresponded to the region of Sn_2S_3 phase. **c** HRTEM image taken from the outer region of the film (marked with *2* in **a**). It shows that the SnO_2 phase distributed on the outer region of the Sn_2S_3 phase. **d** Cross-sectional EDS line-scan profiling spectra of Si, Sn, S, and O elements taken from the film (as shown with a *red line* in **a**)

SnO_2 (101). To further confirm the favorable formation of the Sn_2S_3–SnO_2 layered heterostructure through the annealing of the Sn_2S_3 thin film in ambient air, the spatial distributions of the atomic composition across the Sn_2S_3–SnO_2 film were obtained using a nanoprobe EDS line-scan profiling analysis (Fig. 3d). The Sn signal was homogeneously distributed over the measured region. By contrast, an O signal and an S signal with a clear intensity drop were observed in the outer region of the film, showing that the outer region of the film was mainly composed of Sn and O elements, and the internal region of the film consisted of Sn and S elements. The TEM analyses revealed that a well-layered Sn_2S_3–SnO_2 heterostructure film was formed when the Sn_2S_3 film was treated using the described postannealing procedure in ambient air.

The photoassisted gas-sensing properties of the Sn_2S_3 film with and without postannealing were measured by recording the change in electrical resistance on exposure to various NO_2 gas concentrations. Figure 4a, b shows the dynamic electrical resistance variations of the Sn_2S_3 film and Sn_2S_3–SnO_2 heterostructure film on exposure to 0.2–2.5 ppm of NO_2 gases under light illumination at room temperature. The electrical resistance of the *n*-type Sn_2S_3 film under light illumination was nearly unchanged and maintained at an electrical resistance value of approximately 660 kΩ on exposure to the various NO_2 gas concentrations. The Sn_2S_3 film in this work was inactive when detection of oxidizing NO_2 gas under light illumination at room temperature was attempted. The possible reasons for the inactive gas-sensing responses of the Sn_2S_3 film under light irradiation might be associated with the sensor operating at room temperature, and the measuring system did not provide sufficient thermal energy for NO_2 gas molecules to overcome the barriers to adsorb onto the surface of the Sn_2S_3 during the gas-sensing test. Moreover, a high recombination rate of photoexcited carriers might have occurred in the Sn_2S_3 crystallites, which would not have efficiently provided sufficient free electrons on the surfaces of the sheet-like

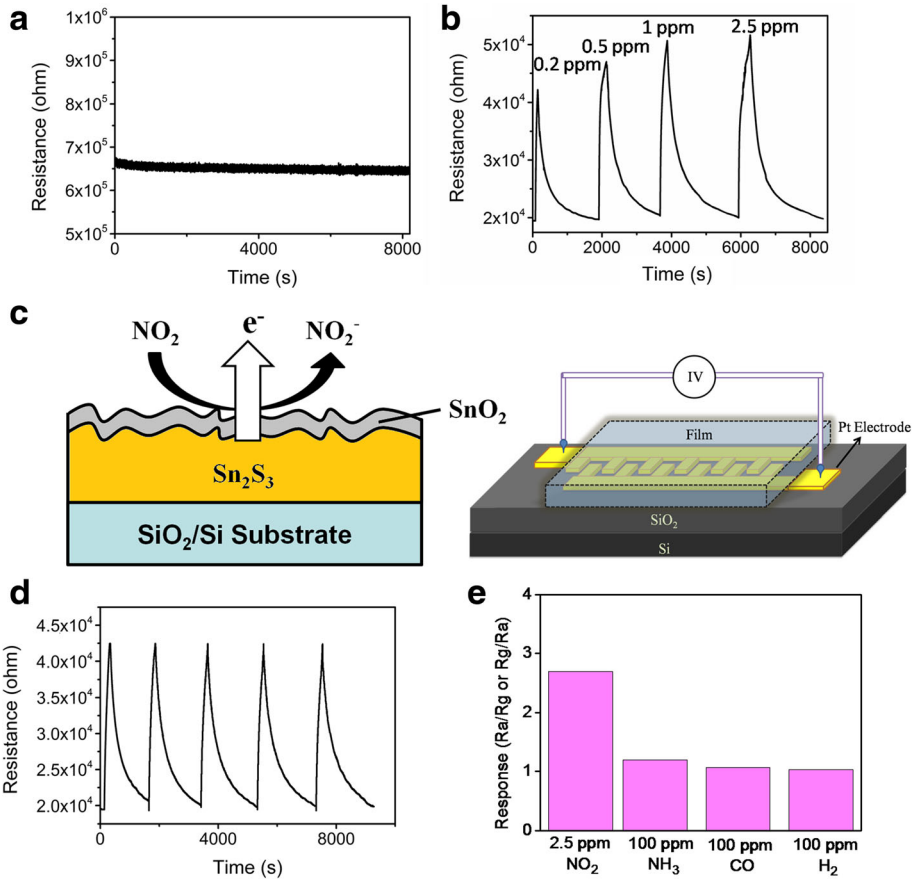

Fig. 4 **a** Dynamic electrical resistance variation curves of the Sn_2S_3 thin film on exposure to various NO_2 gas concentrations (0.2–2.5 ppm) under light irradiation. **b** Dynamic electrical resistance variation curves of the Sn_2S_3–SnO_2 thin film on exposure to various NO_2 gas concentrations (0.2–2.5 ppm) under light irradiation. **c** Schematics of the Sn_2S_3–SnO_2 thin film surface reaction with NO_2 gas molecules and gas sensor device. **d** Cyclic gas-sensing response curves of the Sn_2S_3–SnO_2 thin film on exposure to 0.2 ppm NO_2 gas under light irradiation. **e** The gas-sensing responses of the Sn_2S_3–SnO_2 thin film on exposure to various test gases

Sn_2S_3 crystallites under light illumination. These factors might account for the observed lack of clear oxidizing gas-sensing responses of the sheet-like Sn_2S_3 film under light irradiation at room temperature. By contrast, a clear gas-sensing behavior was observed for the Sn_2S_3–SnO_2 heterostructure thin film toward various NO_2 gas concentrations (Fig. 4b). Schematics of NO_2 gas-sensing reaction on the surface of the heterostructure thin film and gas sensor device are illustrated in Fig. 4c. The initial electrical resistance of the Sn_2S_3–SnO_2 heterostructure thin film under illumination was approximately 19 kΩ. When NO_2 gas was introduced into the test chamber, the measured electrical resistance value of the heterostructure thin film showed a visible increase. Moreover, the cyclic gas-sensing response test for the Sn_2S_3–SnO_2 heterostructure thin film on exposure to 0.2 ppm NO_2 was conducted five times (Fig. 4d). The high repeatability of the gas-sensing response curves revealed that the Sn_2S_3–SnO_2 heterostructure thin film is highly reliable for detecting NO_2 gas under light illumination at room temperature. Notably, the gas-sensing responses of the Sn_2S_3–SnO_2 heterostructure thin film are inactive on exposure to other test gases under light illumination at room temperature (Fig. 4e). The substantial improvement of the oxidizing gas-sensing responses of the Sn_2S_3 film with a moderate postannealing procedure is attributable to the energy band structure of the Sn_2S_3–SnO_2 heterostructure. The work function of Sn_2S_3 is approximately 4.13 eV and that of SnO_2 is approximately 4.9 eV [20, 21]. The work function of Sn_2S_3 is smaller than that of SnO_2; it can be assumed that the interface of SnO_2–Sn_2S_3 is crucial to improving the spatial separation of photoexcited carriers under light illumination. A schematic of the energy-band structure of the Sn_2S_3–SnO_2 heterostructure thin film is illustrated in Fig. 5. A noticeable photoexcited charge transfer between the Sn_2S_3 and SnO_2 was expected. The efficient spatial charge separation prolonged the lifetime of the charges and might have increased the electron density on the surfaces of the sheet-like Sn_2S_3–SnO_2 heterostructure thin film [22]. The formation of the marked electron accumulation layer on the SnO_2 side of the SnO_2–Sn_2S_3 heterostructure was crucial to observing the enhanced gas-sensing properties of the Sn_2S_3–SnO_2 heterostructure in this work. During the gas-sensing process, the electrical resistance increase can be associated with surface-controlled processes and explained by the capturing of free electrons from the surfaces of the *n*-type semiconductors by adsorbed oxidizing NO_2 gas molecules [23, 24]. Such adsorbed NO_2 gas molecules could capture the electrons from the SnO_2 surface of the heterostructure thin film and might have engendered the variation of the depletion layer thickness at the heterointerfaces, resulting in the increased electrical resistance of the sample. This indicated that the higher concentration of electrons on the surfaces of the Sn_2S_3–SnO_2 heterostructure thin film compared with that on the Sn_2S_3 thin film surface can yield a greater opportunity for reaction with NO_2 gas molecules under light illumination at room temperature. Furthermore, the rugged surface of the sheet-like surface morphology of the Sn_2S_3–SnO_2 thin film is more favorable for NO_2 gas molecules adsorption than that of the Sn_2S_3 film. A marked electrical resistance variation of the Sn_2S_3–SnO_2 heterostructure thin film during the oxidizing gas-sensing tests was expected. Notably, the enhancement of gas-sensing properties of the CdS nanowires under light illumination at room temperature was demonstrated in a previous study through the formation of CdS–ZnO heterostructures; the effective interfacial transport of excess carriers contributed to the improved gas-sensing responses [25]. Moreover, in another study, rod-like WO_3-based heterostructures demonstrated improved conductivity, specific electron transfer, and increased gas adsorption compared with those of the single constituent counterpart; these factors contribute to their enhanced light-driven gas-sensing responses to NO_2 gas [26]. Therefore, the suitable band structure of the Sn_2S_3–SnO_2 heterostructure thin film and a rugged surface contributed to the substantial photoassisted room-temperature NO_2 gas-sensing responses of the Sn_2S_3–SnO_2 heterostructure thin film on exposure to low concentrations of NO_2 gases.

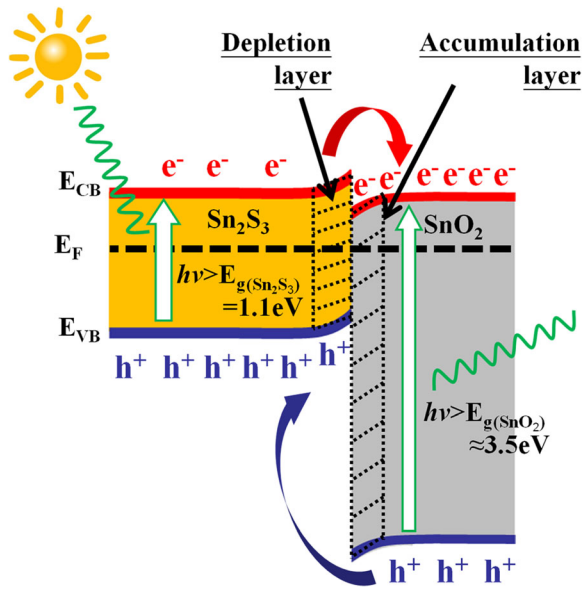

Fig. 5 Band alignment of the Sn_2S_3–SnO_2 thin film under light irradiation

Conclusions

In summary, highly (111)-oriented Sn_2S_3 semiconductor thin films with a sheet-like surface were grown through RF sputtering. The as-synthesized Sn_2S_3 semiconductor

thin films were subsequently treated using postthermal annealing in ambient air at 400 °C. SEM analysis revealed that the surfaces of the Sn_2S_3 thin films were roughened after postannealing in ambient air. Both XRD and TEM analyses indicated that the Sn_2S_3–SnO_2 heterostructure thin films were formed through the formation of the SnO_2 phase on the surfaces of the Sn_2S_3 thin films. By contrast, the Sn_2S_3–SnO_2 heterostructure thin films exhibited visible photoassisted room-temperature gas-sensing responses to low NO_2 gas concentrations. The substantially improved photoassisted room-temperature NO_2 gas-sensing responses of the Sn_2S_3 thin films through facile thermal annealing is attributable to the increased surface roughness and enhanced spatial carrier separation efficiency of the Sn_2S_3–SnO_2 heterostructure thin films.

Abbreviations

EDS: Energy-dispersive X-ray spectrometer; HRTEM: High-resolution transmission electron microscopy; SEM: Scanning electron microscopy; XRD: X-ray diffraction

Acknowledgements

This work is supported by the Ministry of Science and Technology of Taiwan (Grant No. MOST 105-2628-E-019-001-MY3).

Authors' Contributions

YCL designed the experiments and drafted the manuscript. TWL and CCW carried out the sample preparations, material analyses, and characterization tests. All authors read and approved the final manuscript.

Competing Interests

The authors declare that they have no competing interests.

Received: 21 September 2016 Accepted: 4 November 2016
Published online: 16 November 2016

References

1. Zhu HL, Yang DR, Zhang H (2006) Hydrothermal synthesis, characterization and properties of SnS nanoflowers. Mater Lett 60(21-22):2686–2689
2. Yue GH, Wang W, Wang LS, Wang X, Yan PX, Chen Y, Peng DL (2009) The effect of anneal temperature on physical properties of SnS films. J Alloy Compd 474(1-2):445–449
3. Ben Haj Salah H, Bouzouita H, Rezig B (2005) Preparation and characterization of tin sulphide thin films by a spray pyrolysis technique. Thin Solid Films 480-481:439–442
4. Srinivasa Reddy T, Santhosh Kumar MC (2016) Effect of substrate temperature on the physical properties of co-evaporated Sn_2S_3 thin films. Ceram Int 42(10):12262–12269
5. Güneri E, Göde F, Boyarbay B, Gümüş C (2012) Structural and optical studies of chemically deposited Sn_2S_3 thin films. Mater Res Bull 47(11):3738–3742
6. Sanchez-Juarez A, Ortiz A (2002) Effects of precursor concentration on the optical and electrical properties of Sn_XS_Y thin films prepared by plasma-enhanced chemical vapour deposition. Semicond Sci Technol 17:931
7. Liang YC, Cheng YR, Hsia HY, Chung CC (2016) Fabrication and reducing gas detection characterization of highly-crystalline p-type zinc chromite oxide thin film. Appl Surf Sci 364:837–842
8. Liang YC, Deng XS (2014) Microstructure evolution and optical properties of c-axis-oriented ZnO thin films incorporated with silver nanoisland layers. Ceram Int 40(1):1687–1692
9. Liang YC, Zhong H, Liao WK (2013) Nanoscale crystal imperfection-induced characterization changes of manganite nanolayers with various crystallographic textures. Nanoscale Res Lett 8:345–351
10. Yu L, Guo F, Liu S, Yang B, Jiang Y, Qi L, Fan X (2016) Both oxygen vacancies defects and porosity facilitated NO_2 gas sensing response in 2D ZnO nanowalls at room temperature. J Alloy Compd 682:352–356
11. Wang L, Dou H, Loua Z, Zhang T (2013) Encapsuled nanoreactors (Au@SnO_2): a new sensing material for chemical sensors. Nanoscale 5:2686–2691
12. Lou Z, Li F, Deng J, Wang LL, Zhang T (2013) Branch-like hierarchical heterostructure (α-Fe_2O_3/TiO_2): a novel sensing material for trimethylamine gas sensor. ACS Appl Mater Interfaces 5:12310–12316
13. Wang L, Ng WB, Jackman AJ, Cho NJ (2016) Graphene-functionalized natural microcapsules: modular building blocks for ultrahigh sensitivity bioelectronic platforms. Adv Funct Mater 26:2097–2103
14. Cui J, Shi L, Xie T, Wang D, Lin Y (2016) UV-light illumination room temperature HCHO gas-sensing mechanism of ZnO with different nanostructures. Sens Actuators B: Chem 227:220–226
15. Chen H, Liu Y, Xie C, Wu J, Zeng D, Liao Y (2012) A comparative study on UV light activated porous TiO_2 and ZnO film sensors for gas sensing at room temperature. Ceram Int 38(1):503–509
16. Zou Z, Qiu Y, Xie C, Xu J, Luo Y, Wang C, Yan H (2015) CdS/TiO_2 nanocomposite film and its enhanced photoelectric responses to dry air and formaldehyde induced by visible light at room temperature. J Alloy Comp 645:17–23
17. Park S, An S, Mun Y, Lee C (2013) UV-enhanced NO_2 gas sensing properties of SnO_2-Core/ZnO-shell nanowires at room temperature. ACS Appl Mater Interfaces 5:4285–4292
18. Hou YQ, Zhuang DM, Zhang G, Zhao M, Wu MS (2003) Influence of annealing temperature on the properties of titanium oxide thin film. Appl Surf Sci 218(1-4):98–106
19. Liang YC, Hu CY, Liang YC (2012) Crystallographic phase evolution of ternary Zn–Ti–O nanomaterials during high-temperature annealing of ZnO–TiO_2 nanocomposites. CrstEngComm 14(17):5579–5584
20. Burton L (2014) Phase stability and composition of tin sulfide for thin-film solar cells, Thesis (Doctor of Philosophy (PhD)). University of Bath.
21. Liu J, Dai M, Wang T, Sun P, Liang X, Lu G, Shimanoe K, Yamazoe N (2016) Enhanced gas sensing properties of SnO_2 hollow spheres decorated with CeO_2 nanoparticles heterostructure composite materials. ACS Appl Mater Interfaces 8(10):6669–6677
22. Wu P, Sun T, Dai Y, Sun Y, Ye Y, Dai L (2011) Novel type-II Zn_3P_2/ZnO core/shell nanowires: synthesis, characteristic, and photoluminescence properties. Cryst Growth Des 11(5):1417–1421
23. Liang YC, Liu SL (2015) Structure-dependent gas detection ability of clustered ZnS crystallites with heterostructure and tube-like architecture. Acta Mate 88:245–251
24. Liang YC, Cheng YR (2015) Combinational physical synthesis methodology and crystal features correlated with oxidizing gas detection ability of one-dimensional ZnO–VOx crystalline hybrids. CrstEngComm 17:5801–5807
25. Zhai J, Wang L, Wang D, Li H, Zhang Y, He DQ, Xie T (2011) Enhancement of gas sensing properties of CdS nanowire/ZnO nanosphere composite materials at room temperature by visible-light activation. ACS Appl Mater Interfaces 3(7):2253–2258
26. An X, Yu JC, Wang Y, Hu Y, Yu X, Zhang G (2012) WO_3 nanorods/graphene nanocomposites for high-efficiency visible-light-driven photocatalysis and NO_2 gas sensing. J Mater Chem 22:8525–8531